International Journal of Pharmaceutics: X 5 (2023) 100147

Contents lists available at ScienceDirect

International Journal of Pharmaceutics: X

journal homepage: www.sciencedirect.com/journal/international-journal-of-pharmaceutics-x

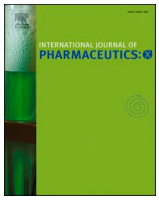

Synergistic effect of doxorubicin lauroyl hydrazone derivative delivered by α-tocopherol succinate micelles for the treatment of glioblastoma

Mingchao Wang [a], Alessio Malfanti [a], Chiara Bastiancich [a,b,c], Véronique Préat [a,*]

[a] Université Catholique de Louvain, Louvain Drug Research Institute, Advanced Drug Delivery and Biomaterials, Brussels, Belgium
[b] Aix-Marseille Univ, CNRS, INP, Inst Neurophysiopathol, Marseille, France
[c] Department of Drug Science and Technology, University of Turin, Turin, Italy

ARTICLE INFO

Keywords:
Glioblastoma
Micelles
α-Tocopherol succinate
Doxorubicin
Drug delivery
Combination therapy

ABSTRACT

We hypothesized that tocopherol succinate (TOS) and D-α-tocopherol polyethylene2000 succinate ($TPGS_{2000}$) micelles could work as a drug delivery system while enhancing the anti-cancer efficacy of doxorubicin lauryl hydrazone derivative ($DOXC_{12}$) for the treatment of glioblastoma. The $DOXC_{12}$-TOS-$TPGS_{2000}$ micelles were formulated with synthesized $DOXC_{12}$ and $TPGS_{2000}$. They showed a high drug loading of hydrophobic $DOXC_{12}$ (29%), a size of <100 nm and a pH sensitive drug release behaviour. *In vitro*, fast uptake of $DOXC_{12}$-TOS-$TPGS_{2000}$ micelles by GL261 cells was observed. For cytotoxicity, $DOXC_{12}$-TOS-$TPGS_{2000}$ micelles were evaluated on two glioblastoma cell lines and showed synergism between $DOXC_{12}$ and TOS-$TPGS_{2000}$. The higher cytotoxicity of $DOXC_{12}$-TOS-$TPGS_{2000}$ micelles was mainly caused by necrosis. The $DOXC_{12}$-TOS-$TPGS_{2000}$ micelles seem to be a promising delivery system for enhancing the anticancer efficacy of doxorubicin in glioblastoma (GBM).

1. Introduction

Glioblastoma (GBM) is a highly malignant primary brain tumor. The median survival time remains less than two years with current "gold standard" therapy that generally includes surgery, radiotherapy plus oral chemotherapy with temozolomide (Stupp et al., 2005). Several treatment challenges explain the low outcome of GBM therapies: 1) the anatomical location of the tumor in the brain and the wide cell infiltration in the brain parenchyma of GBM cells often impede a complete surgical resection and lead to the development of recurrence; 2) extensive cellular and genetic heterogeneity of GBM tumor also impairs the therapeutic outcome of the treatment; 3) the blood-brain barrier limits the access of most chemotherapeutic agents to the tumor limiting the number of drugs that can be used to defeat GBM (Bianco et al., 2017). The complexity of the brain tissue and the continuous crosstalk between tumor cells and the other components of the microenvironment also direct cancer cell fate and response to treatment (Robertson et al., 2019). In >90% of clinical cases, the tumor recurrence arises within a 2 cm region of the resected margin in the macroscopically normal peritumoral zone (Dejaegher and De Vleeschouwer, 2017). Unresectable tumors, such as midline/diencephalic or brainstem tumors, often indicate an overall more aggressive biology leading to treatment failure because of the inefficient therapeutic concentration at the tumor site (Beiko et al., 2014). This suggests that localized drug delivery of drugs directly into the tumor bed or tumor resection cavity would be a promising scenario for treating GBM. Local brain delivery allows the bypass of the BBB and the reduction of systemic toxicity while guaranteeing the therapeutic drug concentrations at the tumor site (Bastiancich et al., 2021). The only approved local treatment for GBM is the carmustine-loaded wafer Gliadel® (Ashby et al., 2016). However, fast drug release and local side effects (*e.g.* seizures, intracranial hypertension, meningitis, cerebral edema, impaired neurosurgical wound healing, wafer migration, etc) limit its clinical use (Bota et al., 2007; Juratli et al., 2013). Therefore, various studies have been focusing on the development of more effective and safe local treatments to improve the current clinical dilemma.

Doxorubicin (DOX) is an anthracycline drug that can induce topoisomerase II poisoning by trapping this enzyme at the cleavage site resulting in double-strand DNA breaks and, thus, cell death (Cortes-Funes and Coronado, 2007; Gewirtz, 1999). It has been widely used for the treatment of various solid tumors, including breast cancer, lung cancer, gastric cancer, ovarian cancer, *etc.* (Ashby et al., 2016; Weiss et al., 1986). In addition, DOX significantly extends survival of glioma-bearing rats and glioma-bearing patients by intralesional administration (Lesniak et al., 2005; Voulgaris et al., 2002). In general, local treatment

* Corresponding author.
E-mail address: veronique.preat@uclouvain.be (V. Préat).

https://doi.org/10.1016/j.ijpx.2022.100147
Received 13 December 2022; Accepted 16 December 2022
Available online 21 December 2022

requires high concentration of therapeutics at the tumor site, which inevitably increases the risk of local side effects and toxicity in the surrounding healthy tissue. Instead of giving a high dose of DOX that could lead to neurotoxicity, a synergistic effect of lower dose of drugs in combination might be a promising approach for enhancing anti-cancer efficacy.

α-tocopherol polyethylene1000 succinate (TPGS, 1.0 kDa) has been widely studied for drug delivery. It is synthesized by the esterification of a Vitamin E derivative, tocopherol succinate (TOS) with hydroxyl moiety of polyethylene glycol (PEG) chain (Golwala et al., 2020; Puig-Rigall et al., 2017). TOS and TPGS are approved by regulatory agencies as biocompatible pharmaceutical solubilizers and absorption enhancers for many poorly water-soluble drugs, respectively (Duhem et al., 2014; Muthu et al., 2012). In addition, they can induce tumor cell apoptosis and inhibit tumor growth in several tumors *in vitro* and *in vivo* (Constantinou et al., 2008; Duhem et al., 2014). In particular, it has been reported that the combination of DOX and α-tocopherol derivatives shows synergism in breast and colon cancer cells (Danhier et al., 2014). The synergism effect of TPGS is primarily attributed to the increased accumulation of DOX into the cells by inhibition of efflux pump P-glycoprotein (P-gp) (Guo et al., 2013). Moreover, amphiphilic TPGS can self-assemble into nano-sized micelles in aqueous media upon reaching the critical micellar concentration (CMC). Micelles are defined as self-assembled nanostructures formed by amphiphilic molecules in an aqueous system with a hydrophobic core inside. (Kazunori et al., 1993) These micelles can solubilize and protect hydrophobic drugs within their core, keep higher kinetic stability compared to low MW surfactant micelles and mimic aspects of biological transport systems. Vitamin E-based nanomedicines were developed to combine the pharmaceutical properties of both vitamin E and nanomedicines for two purposes: (i) to improve the water solubility of hydrophobic drugs and (ii) to benefit from the anticancer activity of TOS and TPGS and enhance the therapeutic efficiency of anticancer agents.

Here, we formulated self-assembled vitamin E derivatives micelles loaded with a novel doxorubicin-hydrazone derivative ($DOXC_{12}$-TOS-$TPGS_{2000}$ micelles) to develop a local treatment of GBM. We evaluated the formulation by physicochemical characterization, cellular uptake, and *in vitro* cytotoxicity studies to show their ability to enhance the anticancer efficacy of doxorubicin in GBM cell lines. By taking advantage of synthesized acid-sensitive prodrug $DOXC_{12}$ and its combination with TOS and $TPGS_{2000}$ within the same nanocarrier, we showed synergistic activity of this drug delivery system which was able to enhance the cytotoxicity of $DOXC_{12}$ alone toward GBM cells.

2. Material and methods

2.1. Synthesis of Doxorubicin lauryl hydrazone derivative ($DOXC_{12}$)

The synthesis of $DOXC_{12}$ was carried out according to a modified procedure reported in the literature (Malfanti et al., 2022). Briefly, doxorubicin hydrochloride (Chemieliva, China) (100 mg, 0.17 mmol, 1.0 eq) and dodecanoic hydrazide (ChemCruz, Netherlands) (53.5 mg, 0.25 mmol, 1.5 eq) were dissolved in methanol in a round-bottomed flask. Glacial acetic acid (100 ul) (Merck, USA) was added to the suspension and left at 40 °C overnight. The solution was precipitated with diethyl ether (Avantor, USA) and the precipitate was collected by centrifugation at 4000 rpm for 5 min after cooling down in dry ice. The precipitation process was repeated 3 times. The final precipitate was collected and further freeze-dried (Labconco, USA) for 48 h. $DOXC_{12}$ was characterized by ^{1}H NMR and high-performance liquid chromatography (HPLC) using a Shimadzu Prominence system (Shimadzu, Japan). A nucleosil C_{18} column (Macherey-Nagel, Germany) (150 × 4.6 mm; particle size 5 μm) was used to separate the final product. 0.1% of formic acid in acetonitrile and 0.1% of formic acid in water (10%, 0 min; 90%, 13–15 min; 10%, 15–20 min) were used as mobile phases and applied at a gradient mode. The quantification method was set with a detection wavelength of 480 nm at a flow rate of 0.6 ml/min.

Yield: 85% *w*/w ^{1}H NMR (DMSO-d_6): 10.35–10.25 (1H,−NH−N) 8.02–7.88 (2H, -CH- benzyl), 7.75–7.59 (1H, -CH-), 5.82–5.76 (1H, CH-OH), 5.64–5.51 (1H, CH_2-OH), 5.51–5.44 (1H, O-CH-), 5.34–5.25 (1H, O-CH-), 4.47–4.33 (2H, CH_2-OH), 4.08–3.91 (3H, O-CH_3), 3.59–3.52 (1H, O-CH-), 3.19–3.10 (1H, -CH-OH), 2.77–2.76 (-CH-NH_2), 2.28–2.03 (2H , -CH_2-) , 1.32–0.72 (26H, C_{12} chain).

2.2. Synthesis of D-α-tocopherol polyethylene 2000 succinate ($TPGS_{2000}$)

The synthesis of $TPGS_{2000}$ was carried out according to a modified procedure reported in the literature (Danhier et al., 2014). Briefly, α-tocopheryl succinate (TOS) (Sigma, USA) (200 mg, 0.46 mmol, 2.5 eq), α-Methoxy-omega-hydroxy poly(ethylene glycol) (MeO-PEG-OH, 2.0 kDa)(Iris Biotec Gmbh, Germany) (377 mg, 0.46 mmol, 0.19 mmol, 1.0 Equiv) and N-(3-Dimethylaminopropyl)-N′-ethyl carbodiimide hydrochloride (EDC) (Sigma, USA) (181 mg, 0.94 mmol, 5.0 eq) were dissolved in the solution of *N*,*N*-Dimethylformamide (DMF) (Sigma, USA). 4-dimethyl aminopyridine (DMAP) (Sigma, USA) (114.8 mg, 0.94 mmol, 5.0 eq) was used as a catalyst in the reaction. TOS and MeO-PEG-OH solution was mixed under an ice bath and stirred for 30 min. EDC solution was added to the above flask and the reaction occurred overnight. The final precipitate was collected after 3 precipitations in diethyl ether and lyophilized (Labconco, USA) for 48 h.

Yield: 95% *w*/w ^{1}H NMR ($CDCl_3$): 4.26–4.18 (2H, -CH_2-OC), 3.80–3.41 (4H, CH_2-CH_2-O-), 3.40–3.34 (3H, -CH_2-CH_3), 3.30–3.25 (4H, CO-CH_2-CH_2), 3.10–2.90 (12H, -C-CH_3), 2.87–1.00 (30H, lipophilic chain), 0.90–0.75 (12H, -CH_3 lipophilic chain).

2.3. Preparation of $DOXC_{12}$–TOS–$TPGS_{2000}$ micelles

$DOXC_{12}$–TOS–$TPGS_{2000}$ micelles were prepared by a thin-film hydration preparation protocol adapted from previous studies (Danhier et al., 2014). Briefly, $DOXC_{12}$ (20 mg), TOS (20 mg), and $TPGS_{2000}$ (20 mg) were dissolved in methanol. The organic solvent was removed by rotary vacuum evaporation at 60 °C. The formed film was then hydrated with 5 ml of PBS under stirring, incubated at 50 °C for 1 h, and then sonicated for a few minutes. Blank-TOS-$TPGS_{2000}$ micelles were formulated by the same procedure but without adding the $DOXC_{12}$.

2.4. Characterization of $DOXC_{12}$–TOS–$TPGS_{2000}$ micelles

2.4.1. Size and zeta potential

The average micelles size and polydispersity index of $DOXC_{12}$–TOS–$TPGS_{2000}$ micelles and unloaded TOS–$TPGS_{2000}$ micelles were measured by dynamic light scattering and zeta potential was determined by laser Doppler velocimetry using a Zetasizer NanoZS (Malvern Instruments, UK) equipped with a red laser (λ = 633 nm) at a fixed angle of 173° at 25 °C.

2.4.2. Quantitative determinations of $DOXC_{12}$ in $DOXC_{12}$–TOS–$TPGS_{2000}$ micelles

$DOXC_{12}$ was quantified by HPLC as described above. A $DOXC_{12}$ calibration curve was established at concentrations ranging from 1 to 200 μg/ml (correlation coefficient of R^2 = 0.9999, LOD = 2.8 μg/ml, LOQ = 8.4 μg/ml, retention time = 14 min, coefficient of variance < 8.5%). The total amount of $DOXC_{12}$ loaded in the $DOXC_{12}$–TOS–$TPGS_{2000}$ micelles was determined by HPLC after the disruption of micelles in acetonitrile (dilution ratio 1:20). The quantification of micelles was adapted and calculated using the following equations (Danhier et al., 2014):

$$DL\% = \frac{amount\ of\ DOXC_{12}\ in\ the\ micelles}{total\ micelles\ weight\ (DOXC_{12} + TOS + TPGS_{2000})} \times 100 \quad (1)$$

$$EE\% = \frac{amount\ of\ DOXC_{12}\ in\ the\ micelles}{total\ amount\ of\ DOXC_{12}\ initially\ added} \times 100 \quad (2)$$

2.4.3. Drug release study of $DOXC_{12}$ in $DOXC_{12}$–TOS–$TPGS_{2000}$ micelles

The release of DOX and $DOXC_{12}$ from micelles was studied using a dynamic dialysis method (Yang et al., 2019). Briefly, phosphate-buffered saline (10 mM) containing 0.5% Tween-80 with different pH values (acetate buffer 5.0, 6.6, and 7.4) was prepared as release media. 1 ml of $DOXC_{12}$-loaded micelles was placed in a dialysis bag (MWCO 6000–8000) and immersed in 12 ml of buffer medium, with stirring at a speed of 110 rpm at 37 °C. At fixed time points, 1 ml of the external solution was withdrawn and replaced with the same volume of fresh drug release medium. The released DOX and $DOXC_{12}$ were quantified by HPLC as the method mentioned above. The percentage of released drugs in DOX equivalent and $DOXC_{12}$ equivalent was calculated based on the initial drug amount inside the dialysis bag. The analysis was performed at least in triplicate.

2.5. In vitro studies

2.5.1. Cell lines and culture

Mouse glioma GL261 cell line (DSMZ, Germany) and human U-87MG cell line (ATTC, USA) were cultured in Eagle's Minimum Essential Medium (EMEM; ATTC, USA) supplemented with 10% Bovine Fetal Serum (Gibco, Life Technologies USA), 100 U/ml penicillin G sodium and 100 µg/ml streptomycin sulfate (Gibco, Life Technologies, USA). Cells were subcultured in 75 cm^2 culture flasks (Corning® T-75, Sigma-Aldrich, USA) and incubated at 37 °C and 5% CO_2.

2.5.2. Cellular uptake studies

GL261 cells were seeded at 1 × 10^5 cells/well on 24-well plates prefilled with round cover glasses. After 24 h of incubation at 37 °C and 5% CO_2, cells were treated with DOX, $DOXC_{12}$ and $DOXC_{12}$–TOS–$TPGS_{2000}$ micelles (5 µM of $DOXC_{12}$ equivalent) in the dark for 15 min, 1 h, 2 h and 4 h. Medium was removed, and cells were fixed with 2% formaldehyde for 20 min. For the staining of nuclei, cells were treated with 4′,6-Diamidino-2-Phenylindole, Dihydrochloride (DAPI, Thermo Fisher Scientific, USA) for 5 min. The plates were washed multiple times with Milli-Q water and the cover glasses were mounted on microscope slides using the ProLong™ anti-attenuation mounting medium (Invitrogen, Carlsbad, CA, USA). The slides were left overnight at room temperature to dry and stored at 4 °C until further use. Cells were then examined using a fluorescence LSM800 inverted microscope (Zeiss, Germany) with excitation filters at 405 nm (DAPI, blue) and 488 nm ($DOXC_{12}$, green). Fluorescent signal intensity was measured and normalized to the area containing cells using the ImageJ Fiji software (v.1.53f51) for three representative images.

2.5.3. Cytotoxicity of the $DOXC_{12}$ and $DOXC_{12}$–TOS–$TPGS_{2000}$ micelles in GBM cells

In vitro cytotoxicity of $DOXC_{12}$ and DOX was assessed on GL261 cells and U-87MG cells by crystal violet assay (Bastiancich et al., 2017). Cells were seeded at 3–5 × 10^3 cells/well in 96-well plate. For U-87MG cell line wells were previously coated with poly(*D*)lysine (PDL, 0.1 mg/ml per well; Sigma-Aldrich, USA) (Bastiancich et al., 2016). After 24 h, cells were treated with different drug concentrations (between 0.0001 and 5 µM) and incubated for 48 and 72 h ($n = 3$). Cells were fixed with 4% formaldehyde (Carl Roth, Germany) for 30 min and then followed by treatment of crystal violet solution (0.5% in 20% Methanol; Sigma-Aldrich, USA) at room temperature. Plates were rinsed multiple times and dried at room temperature. Finally, samples were solubilized with methanol and the crystal violet absorbance (λ: 560 nm) was read with a MultiSkan EX plate reader (Thermo Fisher Scientific, USA). Data were compared to the untreated group (100% viability). Triton 1% was used as a positive control (0% viability). IC_{50} were calculated by using a nonlinear regression inhibitor *versus* response, variable slope.

A similar method was used to assess the cytotoxicity of $DOXC_{12}$–TOS–$TPGS_{2000}$ micelles on GL261 cells and U-87MG cells. Briefly, cells were seeded at 2–6 × 10^3 cells/well in 96-well plates. After 24 h, wells were treated with different concentrations of $DOXC_{12}$, $DOXC_{12}$–TOS–$TPGS_{2000}$ and blank-TOS–$TPGS_{2000}$ micelles and incubated for 48 and 72 h.

2.5.4. Evaluation of combination index

To investigate the combinatorial potential of the co-delivery of $DOXC_{12}$ and Vitamin E derivatives (TOS-$TPGS_{2000}$ micelles), the combination index (CI) based on the IC_{50} value was calculated and compared using Chou, Ting-Chao equation as follows (Chou, 2010; Li et al., 2016):

$$CI = \frac{IC_{50}(DOXC_{12}\ in\ DOXC_{12} - TOS - TPGS_{2000})}{IC_{50}(DOXC_{12})} + \frac{IC_{50}(TOS - TPGS_{2000}\ in\ DOXC_{12} - TOS - TPGS_{2000})}{IC_{50}(TOS - TPGS_{2000})} \quad (3)$$

IC_{50} refers to the concentration of drug needed to inhibit 50% of tumor cells.

CI defines synergism (CI < 1), additive effect (CI = 1), and antagonism (CI > 1).

2.5.5. Flow cytometry

Apoptosis and necrosis were studied on GL261 cells and U-87MG cells with an Annexin V-FITC/7-amino-actinomycin D (7-AAD) apoptosis kit (BioLegend, USA) following the instruction of the manufacturer. Briefly, 200,000 cells were seeded in 12-well plates and incubated overnight. After that, cells were treated with 0.1 µM of $DOXC_{12}$, $DOXC_{12}$-TOS-$TPGS_{2000}$ micelles and TOS-$TPGS_{2000}$ micelles for 24 h. Cells were harvested by trypsin and washed with cold PBS. Cells were resuspended in Annexin V binding buffer at a concentration of 5 × 10^6 cells/ml and incubated with FITC Annexin V and 7-AAD Viability Staining Solution at room temperature for 15 min in the dark. The cells were analyzed using an LSR Fortessa flow cytometer (BD Biosciences, USA) and FlowJo software (Treestar). Cells in the early and late stages of the apoptotic process were stained with the annexin V-FITC conjugate, while necrotic cells were stained only by 7-AAD. Live cells showed no staining.

2.6. Statistics

All results are expressed as mean ± standard deviation (SD) of three independent experiments. Statistical analysis was performed using GraphPad Prism version 8.0 (GraphPad Software, USA) for unpaired *t*-test and one-way ANOVA. *p*-values<0.05 were considered statistically significant (*$p < 0.05$, **$p < 0.01$, ***$p < 0.001$ and ****$p < 0.0001$). In the experiments, n corresponds to the number of independent experiments performed.

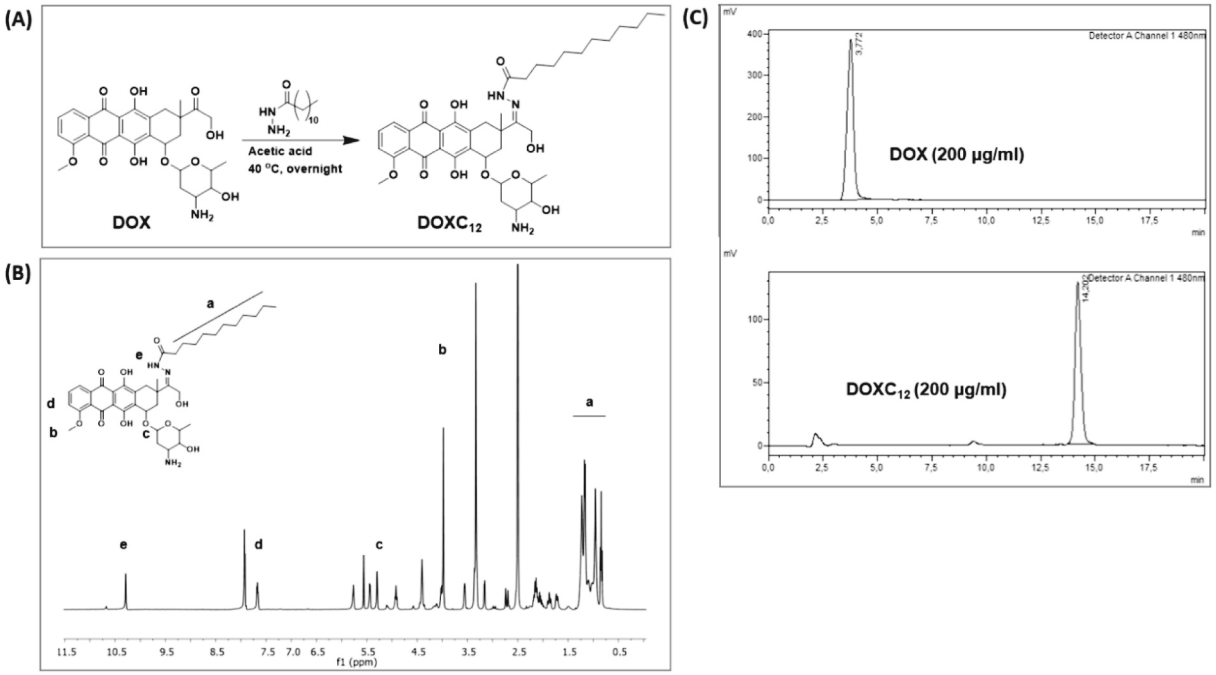

Fig. 1. Scheme of the $DOXC_{12}$ synthesis (A). Identification of $DOXC_{12}$ by ^1H NMR spectrum in DMSO-d_6 (B) and HPLC peak shift (C).

3. Results and discussion

3.1. Synthesis of doxorubicin lauryl hydrazone derivative ($DOXC_{12}$)

To increase the lipophilicity and thus the encapsulation of DOX in the micelles, a lipophilic $DOXC_{12}$ prodrug was synthesized (Fig. 1A). Lauryl hydrazide was conjugated to the ketone group of doxorubicin (C13) to obtain a prodrug with the hydrazone group, $DOXC_{12}$. The synthesis was confirmed by the appearance of highlighted peaks in the ^1H NMR spectrum (Fig. 1B) and the retention time shift in the HPLC spectrum at 14 min (Fig. 1C). Previous results highlighted how C12 chain can enhance the cytotoxicity of drugs in the context of GBM treatment

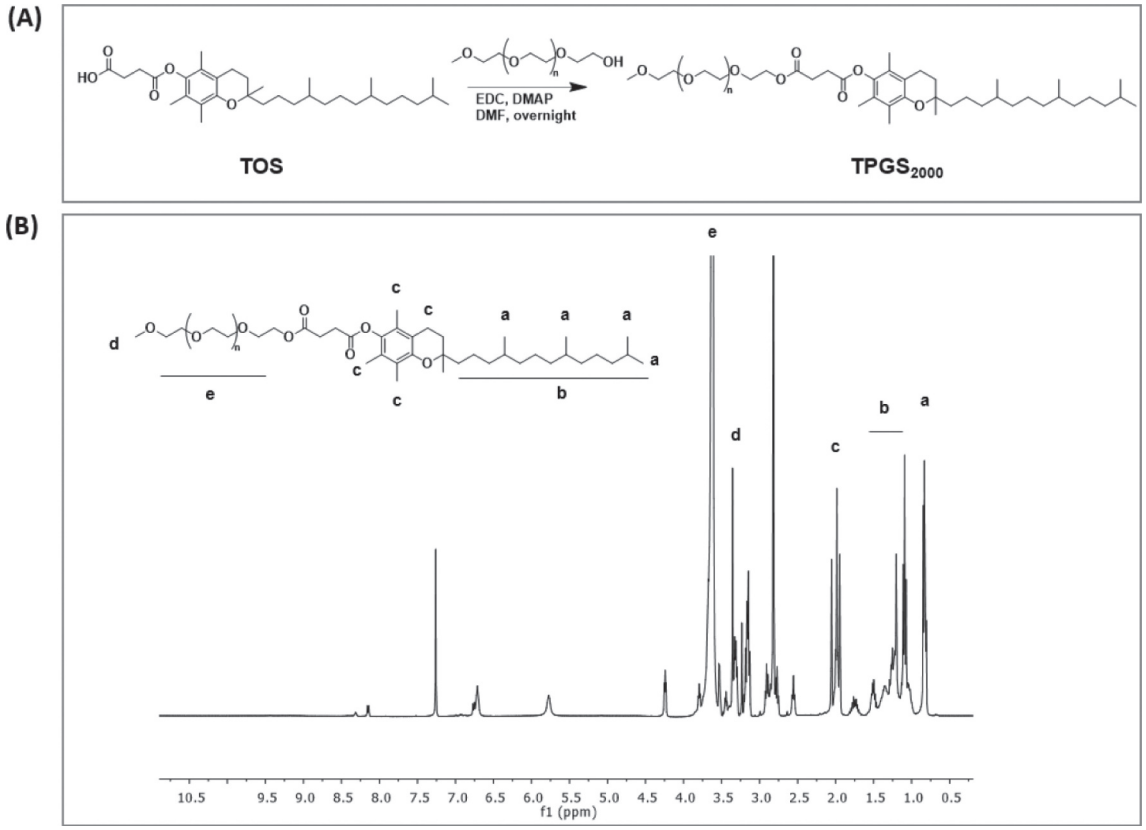

Fig. 2. Synthesis of TOS-TPGS amphiphilic polymer (A). Identification of $TPGS_{2000}$ by ^1H NMR spectrum in $CDCl_3$ (B).

(Bastiancich et al., 2019). The hydrazone-based linking chemistry used to prepare $DOXC_{12}$ has been selected due to its easy preparation method, pH sensitivity allowing DOX release without forming a new chemical entity (Malfanti et al., 2022; Zheng et al., 2019). Moreover, even though Hao *et al* developed $TPGS_{2000}$ micelles loaded with DOX base, $DOXC_{12}$ not only provides higher affinity to the lipophilic core of micelles but also enables DOX release by the breakage of hydrazone bond in acidic pH (Hao et al., 2015). Indeed, following administration, $DOXC_{12}$ could be then converted in DOX either within the tumor microenvironment (pH 6.1–6.8) or intracellularly in the endosomal (pH 5.5–6.0) and lysosomal (pH 4.5–5.0) compartments (Chen et al., 2012).

3.2. Synthesis of D-α-tocopherol polyethylene 2000 succinate ($TPGS_{2000}$)

For the development of micelles, TPGS requires a stable amphiphilic property to form micelles while preserving the anticancer efficacy of parental TPGS (Neophytou et al., 2014; Ruiz-Moreno et al., 2018). In this work, we synthesized $TPGS_{2000}$ by conjugating tocopherol succinate to hydroxyl PEG *via* Steglich esterification (Fig. 2A). The ^1H NMR spectrum (Fig. 2B) shows the presence of an alkyl chain typical of TOS and the methoxy group of PEG. Importantly, we selected this linking chemistry allowing cleavage of the ester bond in the presence of esterase or in acidic conditions, therefore inducing micelles disassembly and release of cargo. The alteration in the length of the PEG segment that esterified with α-tocopherol succinate has an impact on the properties of TPGS and its based polymeric micelles (Tan et al., 2017). Commercially available $TPGS_{1000}$ has been approved as a food supplement, pharmaceutical solubilizer and absorption enhancer by FDA and the European Medicine Agency (EMA), respectively (Danhier et al., 2014). However, as a micellar nanocarrier, the relatively high CMC value (0.2 mg/ml) leads to high potential dissociation in plasma (Yu et al., 1999). Meanwhile, it was reported that the PEG 1000 chain of TPGS is not sufficiently long to ensure prolonged circulation of micelles *in vivo* (Danhier et al., 2014; Mi et al., 2011). Compared to $TPGS_{1000}$, $TPGS_{2000}$ is preferred as a micellar nanocarrier because it can stabilize the molecular structuration of the nanoparticles and avoid aggregation of nanoparticles due to the higher steric hindrance of longer PEG chains. Moreover, by avoiding adhesive interactions with the tumor extracellular matrix, the PEGylated nanocarrier could improve drug diffusion in the brain tissue (Nance et al., 2014).

3.3. Formulation and characterization of $DOXC_{12}$-TOS-$TPGS_{2000}$ micelles

$TPGS_{2000}$ can form micelles spontaneously in an aqueous solution because of its amphiphilicity (Danhier et al., 2014) while TOS is playing an important role as a stabilizer of TPGS-based micelles (Duhem et al., 2014). Therefore, $DOXC_{12}$-TOS-$TPGS_{2000}$ micelles were formulated and characterized by size, zeta potential, encapsulation efficiency, drug loading, and concentration (Table 1).

The reproducibility of the micelles presented in this study was validated by averaged results of three measurements of three distinct batches for each formulation. Compared to the size (113 nm) and the zeta potential (−36 mV) of blank TOS–$TPGS_{2000}$ micelles, $DOXC_{12}$–TOS–$TPGS_{2000}$ micelles showed a smaller size (92 nm) and less negative charge (−6 mV) with a narrow polydispersity index (0.27). This is a drug delivery system consisting of a mixture of $DOXC_{12}$, TOS and $TPGS_{2000}$ (1:1:1, wt%), where hydrophobic TOS contribute to the solubilization of $DOXC_{12}$ while $TPGS_{2000}$ was used to form and stabilize the micellar structuration due to its amphiphilic character. Incorporation of hydrophobic drugs in the micelles can lead to decreased micellar size due to drug-core interaction (Basak and Bandyopadhyay, 2013). In the case of $DOXC_{12}$–TOS–$TPGS_{2000}$ micelles, the phenyl groups, and the alkyl groups of vitamin E derivatives and $DOXC_{12}$ could favorably interact with each other, generating a more compact structure. A size <100 nm would enable the diffusion of micelles in the tumor mass when it comes to intratumoral administration and reach the infiltrating site of GBM cells (Hashizume et al., 2000). The zeta potential is important for the stability of nanoparticles in suspension and is also the major factor in the initial adsorption of nanoparticles onto the cell membrane. A zeta potential value other than −30 mV to +30 mV is generally considered to have a sufficient repulsive force to attain better physical colloidal stability. In unloaded TOS–$TPGS_{2000}$ micelles, TOS presents ionized carboxylic acid groups at the surface of micelles contributing to the highly negative charge at neutral pH (−36 mV), which suggests high stability of the nanocarrier itself. It is worth noting that $DOXC_{12}$–TOS–$TPGS_{2000}$ micelles show decreased surface charge (−6 mV). Indeed, the amine group in $DOXC_{12}$ can neutralize the negative charge of the micelle by interacting with carboxylic acid groups of TOS. Therefore, in the equilibration of TOS and $DOXC_{12}$, we favored achieving a high drug loading rather than a large surface charge considering the steric repulsion of PEG on the surface of micelles can enhance colloidal stability. Interestingly, the high drug loading (29%) of $DOXC_{12}$–TOS–$TPGS_{2000}$ micelles achieved is almost three times the DOX-loaded $TPGS_{2000}$ micelles (DL 9.6%) developed by *Hao et al* (Hao et al., 2015). Meanwhile, Danhier et al. presented a drug concentration of 1.6 mg/ml for the DOX-base based $TPGS_{2000}$ (EE 80%) micelles while the equivalent concentration of DOX in $DOXC_{12}$–TOS–$TPGS_{2000}$ micelles is improved to 2.2 mg/ml (EE 83%, $DOXC_{12}$ eqv 3.4 mg/ml) (Danhier et al., 2014). Indeed, the higher drug loading efficiency and encapsulation efficiency can be explained by the strong hydrophobic interactions established between the alkyl chain (-C12) of $DOXC_{12}$ and the TOS-TPGS-based core of the micelles.

3.4. Drug release study of $DOXC_{12}$ in $DOXC_{12}$–TOS–$TPGS_{2000}$ micelles

Drug release properties of $DOXC_{12}$-TOS-$TPGS_{2000}$ micelles were studied at different pH mimicking the physiological conditions (pH 7.4), the intratumoral pH (pH 6.6) and the *endo*-lysosomal pH (pH 5) where the hydrazone link can be degraded due to the lower pH (Seetharaman et al., 2017; Theillet et al., 2014). Cumulative drug release from drug-loaded micelles at different pH was expressed in $DOXC_{12}$ alone (Fig. 3A), DOX alone (Fig. 3B) and total DOX in equivalents (Fig. 3C). $DOXC_{12}$-TOS-$TPGS_{2000}$ micelles show a time and pH-dependent drug release. This trend can be ascribed to a multiple-step degradation of the system. To investigate the impact of pH on either the release of $DOXC_{12}$ from $DOXC_{12}$-TOS-$TPGS_{2000}$ micelles or the release of DOX from $DOXC_{12}$, statistical analysis (one-way ANOVA) is generated at the endpoint of the study (day 7). At pH 5.0, there is a significantly higher cumulative release of $DOXC_{12}$ compared to pH 6.6 and 7.4 (24 ± 5% *vs* 12 ± 2% and 9 ± 1%) (Fig. 3A, $^{**}p < 0.01$ and $^{***}p < 0.001$). We speculate this acidity decomposed the structure of the self-assembled micelles and released $DOXC_{12}$ while the drug-loaded micelles stay stable at pH 6.6 and 7.4. However, a significantly higher amount of DOX was observed in the medium at pH 6.6 (24 ± 4%) compared to pH 7.4 (15 ± 3%) (Fig. 3B, $^{*}p < 0.05$). Therefore, we speculate that the acidity

Table 1
Physical-chemical characterization of blank TOS-$TPGS_{2000}$ micelles and $DOXC_{12}$-TOS- $TPGS_{2000}$ micelles ($n = 3$; mean ± SD).

Micelles	Size (nm)	PDI	Zeta potential (mV)	EE (%)	DL (%)	$DOXC_{12}$ concentration (mg/ml)
TOS-$TPGS_{2000}$	113 ± 5	0.27 ± 0.04	−36 ± 2	–	–	–
$DOXC_{12}$-TOS-$TPGS_{2000}$	92 ± 6	0.27 ± 0.03	−6 ± 1	83 ± 6	29 ± 1	3.4 ± 0.2

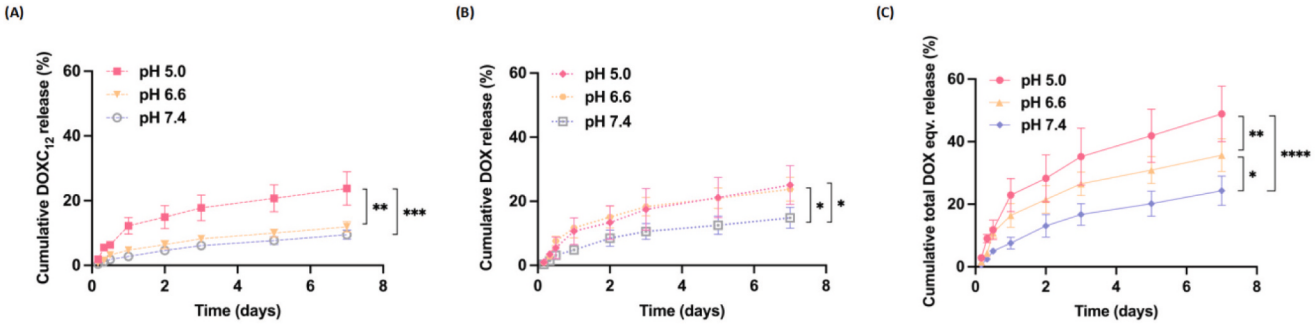

Fig. 3. pH-triggered drug release profile of $DOXC_{12}$-TOS-$TPGS_{2000}$ micelles. Data are presented as the cumulative release of $DOXC_{12}$ (A), cumulative release of DOX (B) and cumulative release of total DOX in equivalent (C) at different pH ($n = 4$; mean ± SD; $^{*}p < 0.05$, $^{**}p < 0.01$, $^{***}p < 0.001$ and $^{****}p < 0.0001$).

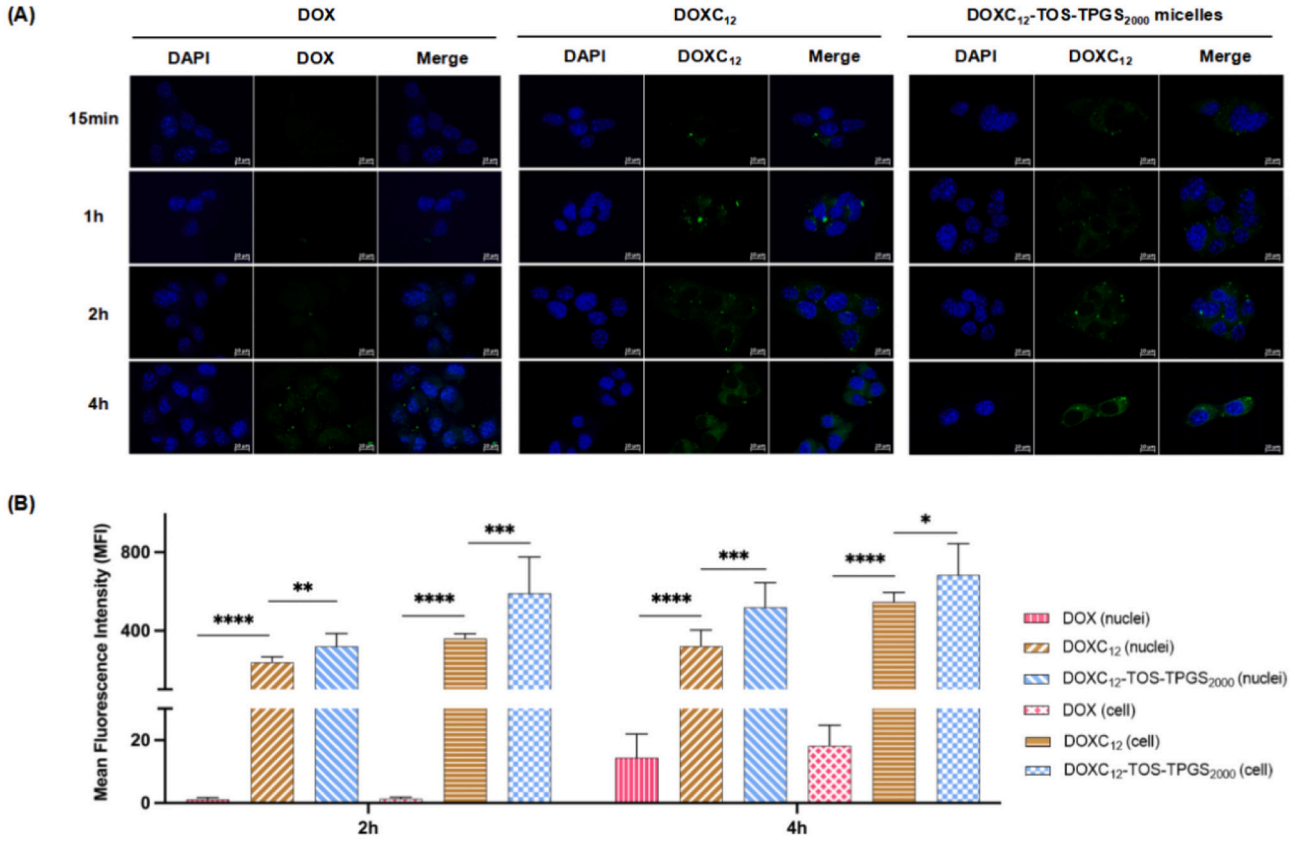

Fig. 4. Cellular uptake of DOX, $DOXC_{12}$ and $DOXC_{12}$–TOS–$TPGS_{2000}$ micelles in GL261 cells. (A) Representative confocal microscopy images of GL261 cell uptake of free DOX, $DOXC_{12}$ and $DOXC_{12}$–TOS–$TPGS_{2000}$ micelles (5 μM of $DOXC_{12}$ equivalent) at 15 min, 1 h, 2 h, and 4 h of incubation. Nuclei were stained with DAPI (DAPI: blue; DOX or $DOXC_{12}$: green). (B) Mean fluorescence intensity in the nuclei and mean cellular fluorescence intensity of GL261 cells treated with DOX, $DOXC_{12}$ and $DOXC_{12}$–TOS–$TPGS_{2000}$ micelles (5 μM of $DOXC_{12}$ equivalent) at 2 h and 4 h of incubation. Data were processed through GraphPad and statistical analysis was obtained by one-way ANOVA comparison ($n = 3$; mean ± SD; $^{*}p < 0.05$; $^{**}p < 0.01$; $^{****}p < 0.0001$). (For interpretation of the references to colour in this figure legend, the reader is referred to the web version of this article.)

at pH 5.0 induces simultaneous cleavage of the hydrazone bond and the structure of the self-assembled micelles, while the acidity at pH 6.6 is able to trigger faster release of DOX from $DOXC_{12}$ compared to neutral pH. Consistently, the highest cumulative drug release of DOX in equivalents from $DOXC_{12}$-TOS-$TPGS_{2000}$ micelles was observed at pH 5.0 (49 ± 9%) followed by pH 6.6 (36 ± 5%) and pH 7.4 (24 ± 5%) (Fig. 3C, $^{*}p < 0.05$, $^{**}p < 0.01$ and $^{****}p < 0.0001$). This observation confirms the pH-sensitivity of the prodrug micelles (Chu et al., 2022; Malfanti et al., 2022).

3.5. Cellular uptake by confocal laser scanning microscopy (CLSM)

The internalization of $DOXC_{12}$–TOS–$TPGS_{2000}$ micelles by GL261 cells was assessed by confocal microscopy taking advantage of the intrinsic fluorescence of DOX. Fast cellular uptake was observed in both groups treated with $DOXC_{12}$ and $DOXC_{12}$–TOS–$TPGS_{2000}$ micelles within 1 h of exposure in GL261 cells compared to DOX treated group (Fig. 4A). We also studied the internalization of drugs in the cells and their nuclei as DOX acts by its anti-cancer efficacy in the cancer cell by

intercalation into DNA. There is a time-dependent way of cellular internalization for DOX, $DOXC_{12}$ and $DOXC_{12}$–TOS–$TPGS_{2000}$ micelles during the first 4 h of exposure (Fig. 4B). Significantly different cellular uptakes between DOX and $DOXC_{12}$ were observed (2 h and 4 h, $^{****}p < 0.0001$). This suggests the conjugation of the lipophilic C12 lauroyl chain on DOX enhanced its capacity to cross the cell membrane. In addition, $DOXC_{12}$–TOS–$TPGS_{2000}$ micelles significantly increased cellular uptake (2 h, $^{***}p < 0.001$; 4 h, $^{*}p < 0.05$) and nuclei uptake (2 h, $^{**}p < 0.01$; 4 h, $^{***}p < 0.001$) of $DOXC_{12}$. Such a difference emphasizes the crucial role of TOS-$TPGS_{2000}$ micelles in the cellular internalization of the drug. Indeed, both the micelles themselves and the intrinsic properties of TOS/TPGS are playing roles in the cell membrane penetration (Wang et al., 2015; Win and Feng, 2006). A study shows that cellular internalization of TPGS-coated nanosystems can be related to the vitamin E moiety that interacts with membrane receptors and induces nanoparticle absorption (Tan et al., 2017). Studies show that pH-sensitive prodrug might convert into the active drug in the endocytic package where there is lower pH compared with the cytosol before entering the nuclei. Endocytosis is the major route of cellular entry as it is for most of bioactive and delivery systems (<250 nm) and the escape of active molecules from the endocytic package into the cytosol or nuclei is the key point of therapeutical efficacy (Foroozandeh and Aziz, 2018; Rajendran et al., 2010). Benefiting from the hydrazone bond in $DOXC_{12}$, $DOXC_{12}$ is released from micelles and migrates in the nuclei.

3.6. *In vitro cytotoxicity of doxorubicin derivative $DOXC_{12}$ and drug-loaded micelles*

In this study, we aimed at increasing the hydrophobicity of DOX while avoiding the loss of its anticancer efficacy. Therefore, $DOXC_{12}$ was synthesized by conjugation of a C_{12} chain to the ketone group of DOX by forming a hydrazone bond. To confirm the anticancer efficacy of this prodrug *in vitro*, we conducted a crystal violet assay on GL261 cells and U-87MG glioma cells for 48 h and 72 h. The cytotoxicity of DOX and $DOXC_{12}$ were time and concentration-dependent (Fig. 5 A, B, D and E). DOX induced significantly lower IC_{50} values compared to $DOXC_{12}$ at 72 h of treatment in both cell lines ($^{*}p < 0.05$). The GL261 cells appear to be more sensitive than U-87MG cells to the treatment. These results confirm that $DOXC_{12}$ preserved a cytotoxic effect. Indeed, sugar moiety (daunosamine) is an essential component of anthracyclines for their antitumor efficacy. Therefore, modifications of the amino sugar are avoided in this synthesis to prevent a decrease in the cytotoxic activity and modifications of the mode of action, even subcellular distribution (Di Marco et al., 1976; Di Marco et al., 1977). The variation in *in vitro* anticancer efficacy of DOX and $DOXC_{12}$ might be explained by their potentially different subcellular delivery (Fig. 4A).

To understand the anti-cancer potential of the co-delivery of $DOXC_{12}$ and TOS–$TPGS_{2000}$ in the same micelle *versus* single-drug or unloaded micelles, we performed a cytotoxicity assay on GL261 and U-87MG glioma cells using a wide drug concentration range (0.0001–5 μg/ml for $DOXC_{12}$ and $DOXC_{12}$–TOS–$TPGS_{2000}$ micelles and 1–400 μg/ml for TOS–$TPGS_{2000}$ micelles). In the equivalent of $DOXC_{12}$, there is no significant cytotoxicity (IC_{50}) difference after 48 h of treatment exposure for GL261 cells ($DOXC_{12}$–TOS–$TPGS_{2000}$ micelles 0.13 μg/ml *vs* $DOXC_{12}$ 0.36 μg/ml) and U-87MG cells ($DOXC_{12}$–TOS–$TPGS_{2000}$ micelles 0.63 μg/ml *vs* $DOXC_{12}$ 2.12 μg/ml). However, significantly enhanced cytotoxicity of $DOXC_{12}$–TOS–$TPGS_{2000}$ micelles was observed compared to free drug $DOXC_{12}$ in both cell lines at 72 h (($DOXC_{12}$–TOS–$TPGS_{2000}$ micelles 0.01 μg/ml *vs* $DOXC_{12}$ 0.09 μg/ml for GL261 cells; $DOXC_{12}$–TOS–$TPGS_{2000}$ micelles 0.13 μg/ml *vs* $DOXC_{12}$ 0.68 μg/ml for U-87 MG cells) (Fig. 6 A and D, $^{*}p < 0.05$). In the equivalent concentration of TPGS, unloaded TOS–$TPGS_{2000}$ micelles show a cytotoxic effect in both GBM cell lines (48 h IC_{50} = 23.19 μg/ml and 72 h IC_{50} = 15.89 μg/ml for GL261 cells, 48 h IC_{50} = 12.2 μg/ml and 72 h IC_{50} = 15.25 μg/ml for U-87 MG cells). GL261 cells show higher sensitivity than U-87MG cells to the treatment of $DOXC_{12}$, which are in line with the work reported with these two cell line (Malfanti et al., 2022), while U-87MG cells seem to be more sensitive to unloaded TOS–$TPGS_{2000}$ micelles. Following the intrinsic cytotoxicity of TOS–$TPGS_{2000}$ micelles, the effect of $DOXC_{12}$ on the cytotoxicity of TOS-TPGS micelles was compared based on the equivalent of TPGS. It shows that $DOXC_{12}$ can significantly decrease IC_{50} of unloaded TOS-$TPGS_{2000}$ micelles (Fig. 6 B and E, $^{***}p < 0.001$; $^{****}p < 0.0001$) in both cell lines at different time points. Indeed, the intrinsic anticancer efficacy of TOS and TPGS has been reported on various cancer cell lines and synergism was observed in combination with DOX (Duhem et al., 2014). TPGS and TOS have intrinsic anticancer activity, their mechanisms might involve 1) targeting the mitochondria of cancer cells, resulting in the mitochondrial

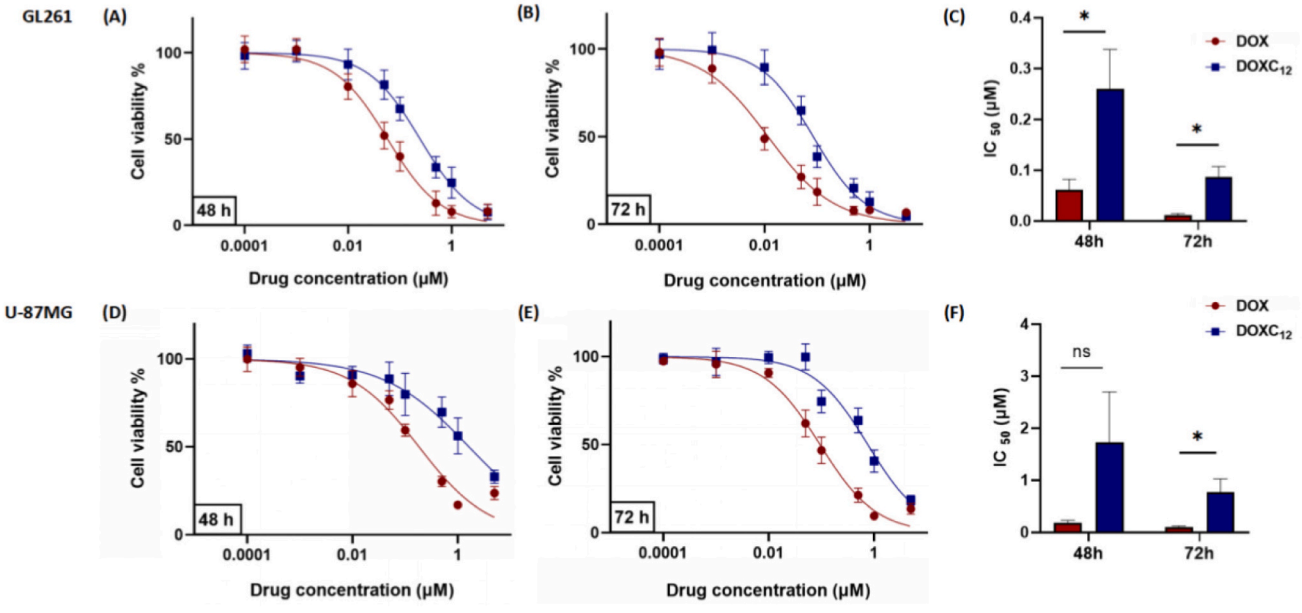

Fig. 5. *In vitro* cytotoxic assay of $DOXC_{12}$ and DOX on glioma cell lines. Cell viability curves of $DOXC_{12}$ and DOX after 48 h and 72 h of incubation in GL261 cells (A, B) and U-87 MG cells (C, D). IC_{50} values of $DOXC_{12}$ and DOX in GL261 cells and U-87 MG cells were expressed in DOX equivalent ($n = 3$; mean ± SD; $^{*}p < 0.05$).

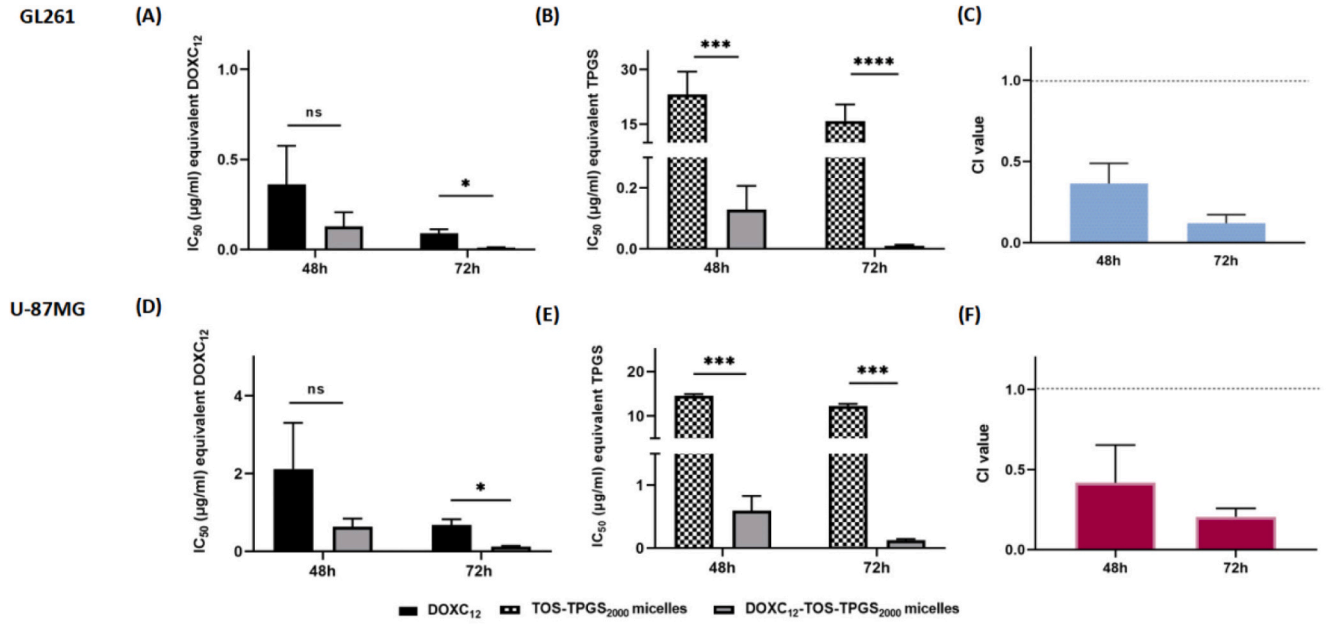

Fig. 6. *In vitro* cytotoxic studies on glioma cells. IC_{50} values of $DOXC_{12}$ and $DOXC_{12}$–TOS–$TPGS_{2000}$ micelles after 48 h and 72 h of incubation in GL261 cells (A) and U-87MG cells (D). Data were expressed in $DOXC_{12}$ equivalent (n = 3; mean ± SD; $^{*}p < 0.05$). IC_{50} values of $DOXC_{12}$–TOS–$TPGS_{2000}$ micelles and unloaded TOS–$TPGS_{2000}$ micelles after 48 h and 72 h of incubation in GL261 cells (B) and U87-MG cells (E). Data were expressed in TPGS equivalent (n = 3; mean ± SD; $^{***}p < 0.001$; $^{****}p < 0.0001$). Combination index (CI) values of $DOXC_{12}$ and unloaded TOS–$TPGS_{2000}$ micelles in GL261 cells (C) and U-87MG cells (F). CI values were calculated with the IC_{50} value of a single treatment based on the Chou-Talalay equation (n = 3; mean ± SD).

destabilization and therefore activating mitochondrial-mediated apoptosis (Neuzil et al., 2007); 2) competitively occupying the ubiquinone-binding sites in the mitochondrial complex II (Constantinou et al., 2008; Neophytou et al., 2014). This leads to the accumulation of electrons which produce reactive oxygen species (ROS) by reacting with molecular oxygen. The cells are driven toward apoptosis because of accumulative oxidative stress.

Based on the principle of a drug combination that combined drugs should not reduce the target efficacy of each other, combination index values between $DOXC_{12}$ and TOS–$TPGS_{2000}$ were calculated in both cell lines at different treatment times (Fig. 6 C and F). CI values are <1 for GL261 cells (48 h CI = 0.4 *vs* 72 h CI = 0.1), similar results are reported in U-87MG cells (48 h CI = 0.4 *vs* 72 h CI = 0.2), indicating the *in vitro* synergism between $DOXC_{12}$ and TOS–$TPGS_{2000}$ in GBM cells. This result indicates the cytotoxicity of $DOXC_{12}$–TOS–$TPGS_{2000}$ micelles is not only the simple sum of the cytotoxicity of $DOXC_{12}$ and TOS–$TPGS_{2000}$. The presence of TOS–$TPGS_{2000}$ enhances the anticancer efficacy of $DOXC_{12}$ *in vitro* in a synergistic manner. This could be explained by the fact that the TPGS nanocarrier inhibited the ATP-dependent doxorubicin efflux pump P-gp, which inducing enhanced the anti-cancer efficacy of DOX at the targeted site (Yang et al., 2018; Zhang et al., 2011). Inhibition of P-gp by TPGS leads to an increased accumulation of drugs, which is consistent with what we observed in the cellular uptake study. Moreover, TPGS was reported as a selective anticancer agent, inducing apoptosis in tumor cells while exhibiting non-toxicity to normal cells and tissues (Duhem et al., 2014; Neuzil et al., 2004). Neophytou et al. observed that TPGS can trigger the apoptotic signaling pathways and induce G1/S cell cycle arrest in breast cancer cells MCF-7 and MDA-MB-231, but no remarkable effect on non-tumorigenic cells MCF-10A and MCF-12F (Neophytou et al., 2014). Therefore, delivery of $DOXC_{12}$–TOS–$TPGS_{2000}$ micelles can be a promising treatment for GBM that selectively kill GBM cells.

3.7. Flow cytometry

To check if the $DOXC_{12}$-TOS-$TPGS_{2000}$ micelles induced higher apoptosis or necrosis than the single treatment, an Annexin V/7-AAD assay was performed. Representative scatter plots with different treatments on both GL261 and U-87MG cells are reported in Fig. 7A. Both apoptosis and necrosis induced by treatment were quantified after 24 h in GL261 and U-87MG cells. Cells treated with $DOXC_{12}$-TOS-$TPGS_{2000}$ micelles showed a significantly higher necrotic cell population percentage than cells treated with $DOXC_{12}$ (Fig. 7B, GL261, 12 ± 3% *vs* 8 ± 4%, $^{*}p < 0.05$; U-87MG, 11 ± 3% *vs* 6 ± 1%, $^{****}p < 0.0001$). However, no difference in apoptosis was observed among different treatments. Several different regulated cell death pathways simultaneously triggered by DOX have been reported, including extrinsic and intrinsic apoptosis, autophagy and necrosis (Meredith and Dass, 2016). Apoptosis is the process of regulated cell death, while necrosis refers to unregulated cell death triggered by chemotherapeutic drugs or other insults (Shin et al., 2015). Indeed, it appears that $DOXC_{12}$-TOS-$TPGS_{2000}$ micelles possess a significantly higher capability of inducing necrosis compared to single treatments in both cell lines. This confirms the fact that the synergistic cytotoxicity of $DOXC_{12}$-TOS-$TPGS_{2000}$ micelles (Fig. 6 C and F) can be a consequence of increased necrotic cell death.

As a drug delivery system, $DOXC_{12}$–TOS–$TPGS_{2000}$ micelles can combine the delivery of the cytotoxic agent with a superior anticancer efficacy mediated by both cargo and nanocarrier as well as increased permeation/accumulation ability. Wang et al. prepared docetaxel-loaded hybrid micelles with DSPE-PEG and TPGS, where TPGS serves as an effective P-gp inhibitor for overcoming multi-drug resistance. The *in vivo* study showed that the hybrid micelles with TPGS can penetrate over 10-fold higher depth in a multi-drug resistant human mouth epidermoid carcinoma KBv tumor spheroid model compared to TPGS-free micelles, indicating TPGS may increase drug permeation in solid

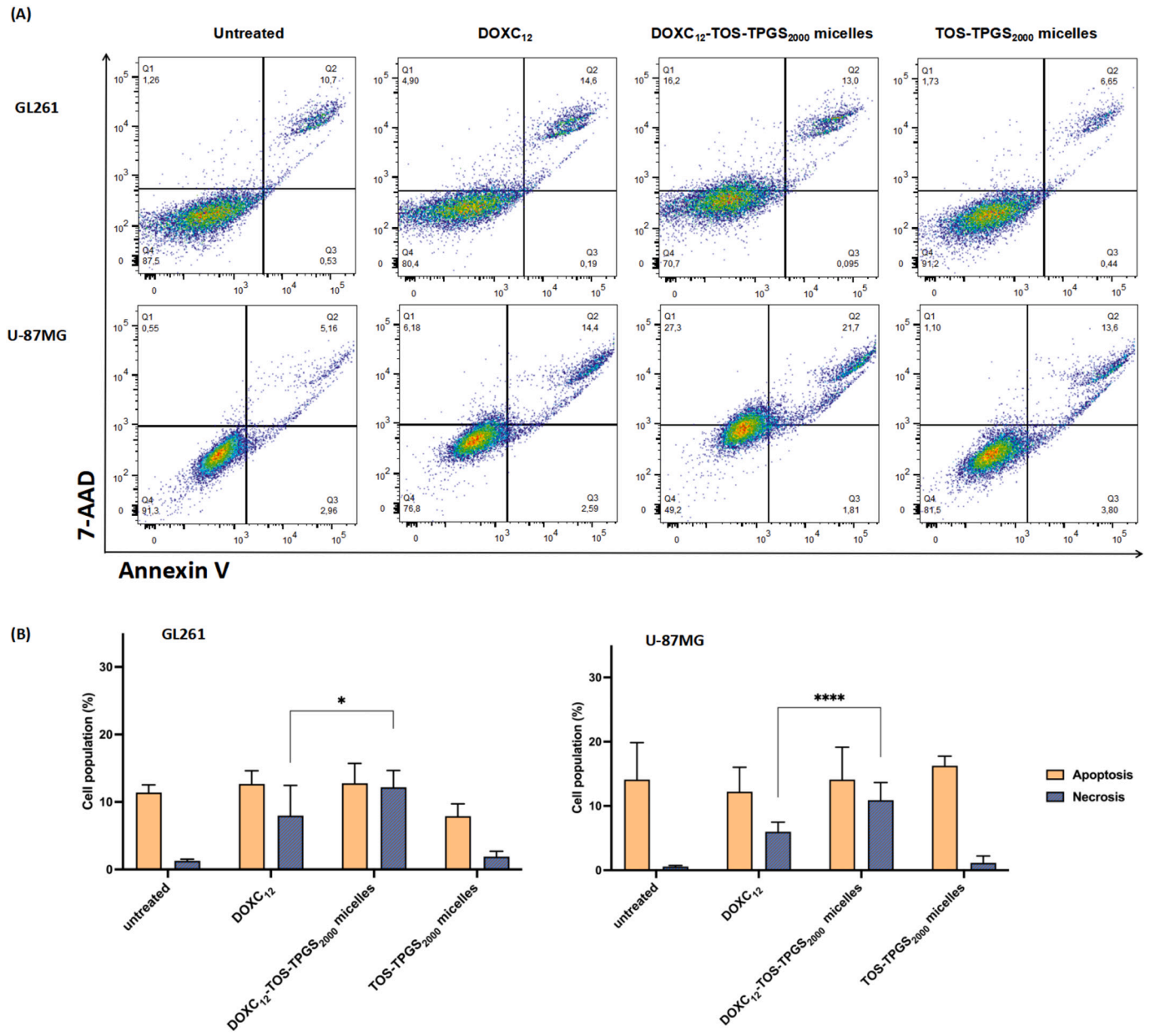

Fig. 7. Annexin V/7-AAD assay after 24 h of incubation on GL261 cells and U-87MG cells with 0.1 μM of $DOXC_{12}$, $DOXC_{12}$-TOS-$TPGS_{2000}$ micelles and TOS-$TPGS_{2000}$ micelles. (A) Representative scatter plots present cell populations divided into four quadrants: healthy cells (lower left), early apoptotic cells (lower right), late apoptotic cells (upper right) and necrotic cells (upper left). (B) Population percentage of the annexin V-positive cells (apoptosis) and 7-AAD-positive but annexin V-negative cells (necrosis) ($n = 3$; mean ± SD; $^{*}p < 0.05$, $^{****}p < 0.0001$).

tumors (Wang et al., 2015). Cao et al. also reported that TPGS can enhance the tumor accumulation of micelles in terms of time, space, and amount (Cao et al., 2016). Interstitial extracellular matrix diffusion was more considered responsible for cell penetration of TPGS than the transcytosis pathway. To maximize its therapeutic efficacy, local administration should be considered for further preclinical studies using this drug-loaded delivery system. For example, convection-enhanced delivery (CED) is a therapeutic local delivery strategy that was developed to increase the drug concentration in the brain by a continuous positive-pressure infusion of the therapeutic agent directly into the brain tumor. Subsequently, it provides interstitial drug distribution over time to kill GBM cells (Lin et al., 2015). Alternatively, a local scaffold loaded with $DOXC_{12}$–TOS–$TPGS_{2000}$ micelles would provide sustained drug release in the GBM resection microenvironment, leading to long-term anti-cancer efficacy.

4. Conclusions

To develop an effective treatment for GBM, we designed $DOXC_{12}$–TOS–$TPGS_{2000}$ micelles with a simple-to-prepare and easy-to-scale-up process. The rationale was based on the anticancer effect of TOS and TGPS and the synergy observed with DOX in other cancers. With synthesized hydrazone-bond containing prodrug $DOXC_{12}$, high encapsulation efficiency and drug loading were achieved in $DOXC_{12}$–TOS–$TPGS_{2000}$ micelles. An appropriate size should enable the system diffusion in the brain (tumor) architecture tissue. A fast and time-dependent accumulation of $DOXC_{12}$ was highlighted when delivering $DOXC_{12}$ in TOS-$TPGS_{2000}$ micelles. The cytotoxicity on two glioma cell lines confirms that i) TOS-$TGPS_{2000}$ micelles exert a cytotoxic effect on GBM cells ii) a synergism is observed between $DOXC_{12}$ and TOS-$TGPS_{2000}$ in GBM cells. The synergistic cytotoxicity is mainly caused by enhanced necrotic cell death. In conclusion, this proof-of-concept study

shows the potential of $DOXC_{12}$–TOS–$TPGS_{2000}$ micelles as drug delivery systems for the local treatments for GBM and, eventually, for other incurable tumors.

Declaration of Competing Interest

The authors declare no conflict of interest.

Data availability

Data will be made available on request.

Acknowledgments

M.W. is supported by the Université Catholique de Louvain and the China Scholarship Council (CSC). A.M. is supported by the Marie Skłodowska-Curie Actions for an Individual European Fellowship under the European Union's Horizon 2020 research and innovation program (grant agreement no. 887609) and by Fonds de la Recherche Scientifique—Fonds National de la Recherche Scientifique (FRS-FNRS) (grant agreement no. 40000747) (Belgium). C.B. is supported by Fondation ARC pour la recherche sur le cancer (grants n. PDF20190509176 and n. ARCPJA12020060002222) and Cancéropôle Provence Alpes Côte d'Azur. V.P. is supported by FRS-FNRS (grant agreements no. 33669945, 40003419).

References

Ashby, L.S., Smith, K.A., Stea, B., 2016. Gliadel wafer implantation combined with standard radiotherapy and concurrent followed by adjuvant temozolomide for treatment of newly diagnosed high-grade glioma: a systematic literature review. World J. Surgical Oncol. 14, 1–15.
Basak, R., Bandyopadhyay, R., 2013. Encapsulation of hydrophobic drugs in Pluronic F127 micelles: effects of drug hydrophobicity, solution temperature, and pH. Langmuir. 29, 4350–4356.
Bastiancich, C., et al., 2016. Anticancer drug-loaded hydrogels as drug delivery systems for the local treatment of glioblastoma. J. Control. Release 243, 29–42.
Bastiancich, C., et al., 2017. Injectable nanomedicine hydrogel for local chemotherapy of glioblastoma after surgical resection. J. Control. Release 264, 45–54.
Bastiancich, C., et al., 2019. Drug combination using an injectable nanomedicine hydrogel for glioblastoma treatment. Int. J. Pharmaceut. 559, 220–227.
Bastiancich, C., et al., 2021. Rationally designed drug delivery systems for the local treatment of resected glioblastoma. Adv. Drug Deliv. Rev. 177, 113951.
Beiko, J., et al., 2014. IDH1 mutant malignant astrocytomas are more amenable to surgical resection and have a survival benefit associated with maximal surgical resection. Neuro-oncology. 16, 81–91.
Bianco, J., et al., 2017. On glioblastoma and the search for a cure: where do we stand? Cell. Mol. Life Sci. 74, 2451–2466.
Bota, D.A., et al., 2007. Interstitial chemotherapy with biodegradable BCNU (Gliadel®) wafers in the treatment of malignant gliomas. Ther. Clin. Risk Manag. 3, 707.
Cao, X., et al., 2016. Diblock-and triblock-copolymer based mixed micelles with high tumor penetration in vitro and in vivo. J. Mater. Chem. B 4, 3216–3224.
Chen, X., et al., 2012. PolyMPC–doxorubicin prodrugs. Bioconjug. Chem. 23, 1753–1763.
Chou, T.-C., 2010. Drug combination studies and their synergy quantification using the Chou-Talalay method. Cancer Res. 70, 440–446.
Chu, S., et al., 2022. Ph-responsive polymer nanomaterials for tumor therapy. Front. Oncol. 12.
Constantinou, C., Papas, A., Constantinou, A.I., 2008. Vitamin E and cancer: an insight into the anticancer activities of vitamin E isomers and analogs. Int. J. Cancer 123, 739–752.
Cortes-Funes, H., Coronado, C., 2007. Role of anthracyclines in the era of targeted therapy. Cardiovasc. Toxicol. 7, 56–60.
Danhier, F., et al., 2014. Vitamin E-based micelles enhance the anticancer activity of doxorubicin. Int. J. Pharmaceut. 476, 9–15.
Dejaegher, J., De Vleeschouwer, S., 2017. Recurring Glioblastoma: a Case for Reoperation? Exon Publications, pp. 281–296.
Di Marco, A., et al., 1976. Relationship between activity and amino sugar stereochemistry of daunorubicin and adriamycin derivatives. Cancer Res. 36, 1962–1966.
Di Marco, A., et al., 1977. Changes of activity of daunorubicin, adriamycin and stereoisomers following the introduction or removal of hydroxyl groups in the amino sugar moiety. Chem. Biol. Interact. 19, 291–302.
Duhem, N., Danhier, F., Préat, V., 2014. Vitamin E-based nanomedicines for anti-cancer drug delivery. J. Control. Release 182, 33–44.
Foroozandeh, P., Aziz, A.A., 2018. Insight into cellular uptake and intracellular trafficking of nanoparticles. Nanoscale Res. Lett. 13, 1–12.
Gewirtz, D., 1999. A critical evaluation of the mechanisms of action proposed for the antitumor effects of the anthracycline antibiotics adriamycin and daunorubicin. Biochem. Pharmacol. 57, 727–741.
Golwala, P., et al., 2020. Effect of cosurfactant addition on phase behavior and microstructure of a water dilutable microemulsion. Colloids Surf. B: Biointerfaces 186, 110736.
Guo, J.Y., Xia, B., White, E., 2013. Autophagy-mediated tumor promotion. Cell. 155, 1216–1219.
Hao, T., et al., 2015. Micelles of d-α-tocopheryl polyethylene glycol 2000 succinate (TPGS 2K) for doxorubicin delivery with reversal of multidrug resistance. ACS Appl. Mater. Interfaces 7, 18064–18075.
Hashizume, H., et al., 2000. Openings between defective endothelial cells explain tumor vessel leakiness. Am. J. Pathol. 156, 1363–1380.
Juratli, T.A., Schackert, G., Krex, D., 2013. Current status of local therapy in malignant gliomas—a clinical review of three selected approaches. Pharmacol. Ther. 139, 341–358.
Kazunori, K., et al., 1993. Block copolymer micelles as vehicles for drug delivery. J. Control. Release 24, 119–132.
Lesniak, M.S., et al., 2005. Local delivery of doxorubicin for the treatment of malignant brain tumors in rats. Anticancer Res. 25, 3825–3831.
Li, H., et al., 2016. Cisplatin and doxorubicin dual-loaded mesoporous silica nanoparticles for controlled drug delivery. RSC Adv. 6, 94160–94169.
Lin, N.U., et al., 2015. Response assessment criteria for brain metastases: proposal from the RANO group. Lancet Oncol. 16, e270–e278.
Malfanti, A., et al., 2022. Design of bio-responsive hyaluronic acid–doxorubicin conjugates for the local treatment of glioblastoma. Pharmaceutics. 14, 124.
Meredith, A.-M., Dass, C.R., 2016. Increasing role of the cancer chemotherapeutic doxorubicin in cellular metabolism. J. Pharm. Pharmacol. 68, 729–741.
Mi, Y., Liu, Y., Feng, S.-S., 2011. Formulation of docetaxel by folic acid-conjugated D-α-tocopheryl polyethylene glycol succinate 2000 (Vitamin E TPGS2k) micelles for targeted and synergistic chemotherapy. Biomaterials. 32, 4058–4066.
Muthu, M.S., et al., 2012. Theranostic liposomes of TPGS coating for targeted co-delivery of docetaxel and quantum dots. Biomaterials. 33, 3494–3501.
Nance, E., et al., 2014. Brain-penetrating nanoparticles improve paclitaxel efficacy in malignant glioma following local administration. ACS Nano 8, 10655–10664.
Neophytou, C.M., et al., 2014. D-alpha-tocopheryl polyethylene glycol succinate (TPGS) induces cell cycle arrest and apoptosis selectively in Survivin-overexpressing breast cancer cells. Biochem. Pharmacol. 89, 31–42.
Neuzil, J., et al., 2004. Vitamin E analogues: a new class of inducers of apoptosis with selective anti-cancer effects. Curr. Cancer Drug Targets 4, 355–372.
Neuzil, J., et al., 2007. Vitamin E analogues as a novel group of mitocans: anti-cancer agents that act by targeting mitochondria. Mol. Asp. Med. 28, 607–645.
Puig-Rigall, J., et al., 2017. Structural and spectroscopic characterization of TPGS micelles: disruptive role of cyclodextrins and kinetic pathways. Langmuir. 33, 4737–4747.
Rajendran, L., Knölker, H.-J., Simons, K., 2010. Subcellular targeting strategies for drug design and delivery. Nat. Rev. Drug Discov. 9, 29–42.
Robertson, F.L., et al., 2019. Experimental models and tools to tackle glioblastoma. Dis. Model. Mech. 12, dmm040386.
Ruiz-Moreno, C., Velez-Pardo, C., Jimenez-Del-Rio, M., 2018. Vitamin E D-α-tocopheryl polyethylene glycol succinate (TPGS) provokes cell death in human neuroblastoma SK-N-SH cells via a pro-oxidant signaling mechanism. Chem. Res. Toxicol. 31, 945–953.
Seetharaman, G., et al., 2017. Design, preparation and characterization of pH-responsive prodrug micelles with hydrolyzable anhydride linkages for controlled drug delivery. J. Colloid Interface Sci. 492, 61–72.
Shin, H.-J., et al., 2015. Doxorubicin-induced necrosis is mediated by poly-(ADP-ribose) polymerase 1 (PARP1) but is independent of p53. Sci. Rep. 5, 1–17.
Stupp, R., et al., 2005. Radiotherapy plus concomitant and adjuvant temozolomide for glioblastoma. N. Engl. J. Med. 352, 987–996.
Tan, S., et al., 2017. Recent developments in d-α-tocopheryl polyethylene glycol-succinate-based nanomedicine for cancer therapy. Drug Deliv. 24, 1831–1842.
Theillet, F.X., et al., 2014. Physicochemical properties of cells and their effects on intrinsically disordered proteins (IDPs). Chem. Rev. 114, 6661–6714.
Voulgaris, S., et al., 2002. Intratumoral doxorubicin in patients with malignant brain gliomas. Am. J. Clin. Oncol. 25, 60–64.
Wang, A.-T., et al., 2015. Roles of ligand and TPGS of micelles in regulating internalization, penetration and accumulation against sensitive or resistant tumor and therapy for multidrug resistant tumors. Biomaterials. 53, 160–172.
Weiss, R.B., et al., 1986. Anthracycline analogs the past, present, and future. Cancer Chemother. Pharmacol. 18, 185–197.
Win, K.Y., Feng, S.-S., 2006. In vitro and in vivo studies on vitamin E TPGS-emulsified poly (D, L-lactic-co-glycolic acid) nanoparticles for paclitaxel formulation. Biomaterials. 27, 2285–2291.
Yang, C., et al., 2018. Recent advances in the application of vitamin E TPGS for drug delivery. Theranostics. 8, 464.
Yang, Y., et al., 2019. A smart pH-sensitive delivery system for enhanced anticancer efficacy via paclitaxel endosomal escape. Front. Pharmacol. 10, 10.
Yu, L., et al., 1999. Vitamin E-TPGS increases absorption flux of an HIV protease inhibitor by enhancing its solubility and permeability1. Pharm. Res. 16, 1812–1817.
Zhang, Y., et al., 2011. Ovarian cancer-associated fibroblasts contribute to epithelial ovarian carcinoma metastasis by promoting angiogenesis, lymphangiogenesis and tumor cell invasion. Cancer Lett. 303, 47–55.
Zheng, Y., et al., 2019. Targeted pharmacokinetics of polymeric micelles modified with glycyrrhetinic acid and hydrazone bond in H22 tumor-bearing mice. J. Biomater. Appl. 34, 141–151.